

# Parameter Extraction and Characteristics Study for Manganese-Type Lithium-Ion Battery

Natthawuth Somakettarin <sup>\*‡</sup>, Tsuyoshi Funaki <sup>\*</sup>

<sup>\*</sup>Division of Electrical, Electronic and Information Engineering, Graduate School of Engineering,  
Osaka University, 2-1 Yamada-oka, Suita, Osaka, 565-0871 Japan  
(natthawuth@ps.eei.eng.osaka-u.ac.jp, funaki@ps.eei.eng.osaka-u.ac.jp)

<sup>‡</sup>Corresponding Author; Natthawuth Somakettarin, 2-1 Yamada-oka, Suita, Osaka, 565-0871 Japan,  
Tel: +81 066 879 7709, Fax: +81 066 879 7713, natthawuth@ps.eei.eng.osaka-u.ac.jp

*Received: 28.01.2015 Accepted: 05.03.2015*

**Abstract-** In this paper, we propose the battery transient response model and parameter extraction method for studying the dynamic behaviors of Manganese-type Lithium-Ion battery. The background knowledge of the battery structure and its operating principle are also concluded. Several aspects of operating conditions, such as charging and discharging operations, environments of terminal currents and temperatures, are considered through the experiments for understanding the battery behaviors. The characteristics of internal effective series resistance, battery capacity, and capacity deterioration to the operational and environmental conditions are also evaluated and analyzed physically. The transient response model and the extracted parameters are validated with a Spice simulation for the practical testing data. The terminal voltage response shows an acceptable conformity for the experiment and simulation to different periods and amplitudes of pulse currents.

**Keywords:** Lithium-Ion, Manganese-type, battery characteristics, parameter extraction, transient response model, capacity deterioration.

## 1. Introduction

In recent years, renewable energy resources, such as solar and wind energy, have been more popularization in this energy crisis decade. They are anticipated as a solution to mitigate the energy problems. In order to utilize the renewable resources efficiently and worthily, the energy storage system (ESS) with battery and their management systems are the key technologies. Rechargeable Lithium-ion (Li-Ion) batteries are being considered as the major solution for the future energy storage system. Due to the prominent characteristics of Li-ion battery (LIB), including high energy density, high power, fast response, low self-discharge rate, and long cycle and calendar life [1], that is why many people are interested and continuously develop in this technology.

In this research, we are focusing on the Manganese-type Li-Ion battery (Mn-LIB) that has several notable characteristics. These are good thermal stability, moderate to high energy density, and the highest nominal voltage per cell when compared with such other types as Lithium Cobalt Oxide (LCO)

and Lithium Iron Phosphate (LFP). These characteristics are suitable for applying in the large-scale ESS. In order to use the energy from battery appropriately, the understanding of nonlinear dynamic characteristics of battery with the operating conditions is indispensable. Based on the previous research [2-4], many articles have studied on the dynamic characteristics and parameter estimation of LIB. However, most of them do not explain the concordance of the results with the physical phenomena. For understanding this Mn-LIB, we conclude an operating principle related to its structure explanation and physically explain the corresponding phenomenon in the results obtained from the experiments.

In this paper, we propose the transient response model for Mn-LIB based on the Randle's equivalent circuit model [5] and explain the meaning of electrical parameters from the equivalent circuit related to the internal chemical reaction processes. The test system and procedure are designed appropriately in our laboratory for studying the dynamic behaviors of Mn-LIB. The measurement technique and evaluation method are also introduced. This test system can also be used to perform the tests for extracting the parameters

of battery, and we propose the parameter extraction and verification methods for this battery type.

The electrical characteristics of this single-cell Mn-LIB in charge and discharge operations at different temperatures and terminal currents (C-rates), and the operating temperature dependency of internal effective series resistance (ESR) are discussed. The battery capacity and capacity deterioration to the operational and environmental conditions are also experimentally evaluated in this paper. These characterizations are used for studying and understanding the behaviors of the Mn-LIB and the applicable limitation in utilizing the linear model of battery.

In addition, the aim of this study is to provide an accurate equivalent circuit model of battery using the practical testing information:

- For understanding and predicting battery behaviors
- For evaluating the operation efficiency and state of charge in several temperature environments
- For designing the large-scale energy management system for renewable energy system

The content details of this paper are organized as follows: The operating principle, the structure, the equivalent circuit model, and related parameters of Mn-LIB are described in Section 2. For Section 3, we propose the test system, the testing procedure, and the parameter extraction method based on the experiment of transient response. The verification of model and extracted parameters is explained in Section 4. Section 5 discusses and evaluates the characteristics results of Mn-LIB for understanding the battery behaviors under various operations and temperatures. Finally, In Section 6, we conclude the summary and future research directions.

## 2. Understanding the Mn-type Li-Ion battery

### 2.1. Operating principle and structure

Understanding of the operating principle and Mn-LIB structure is essential for studying and explaining the physical behaviors that miscellaneously occur inside the battery during operations. In this section, main components and the operating principle inside the Mn-LIB will be explained using the simplified schematic of battery structure as shown in Fig. 1.

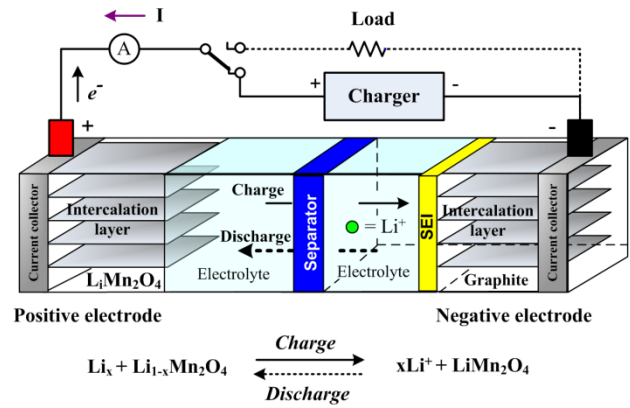


**Fig. 1.** Structure and the overall chemical reaction of Mn-type Li-Ion battery.

Main operating principle for rechargeable Mn-LIB can be divided into 2 processes. They are charging and discharging processes. In charging process, after energizing the rated charging voltage from the charger through the current collector into battery terminals, the electron current is forced to flow through an external circuit from the positive electrode into the negative electrode. Generally, the current collector, which is made from thin aluminium foil for positive side and thin copper foil for negative side, flows current into the cell.

The positive electrode is made from Li-Ion Manganese Oxide ( $\text{LiMn}_2\text{O}_4$ ). This electrode constitutes a porous 3D-spinel crystalline structure, which only allows the Li-Ion insertion or extraction. This type of structure has a good performance in fast charge and discharge operations, high current rupturing capacity and has a low internal resistance property. This structure also gives higher thermal stability for overcharge. That means more safety, less toxicity, and lower cost than the conventional type as the  $\text{LiCoO}_2$  battery [6], [7]. The reaction that Li-Ion is extracted from  $\text{LiMn}_2\text{O}_4$  positive electrode in charging called the oxidation reaction. Li-Ion moves through the electrolyte, separator, into negative electrode inside the battery. At negative electrode, Li-Ion is inserted into the electrode, which is called the reduction reaction. Usually, the negative electrode is made from the carbon-based Lithiated graphite ( $\text{LiC}_6$ ).  $\text{LiC}_6$  has a dominant property in high storage capacity due to its flat potential profile (0-0.3V). On the contrary, for discharging process, when the switch is moved to the load, Li-Ion moves from negative to positive electrode through the electrolyte. At the same time, the electron current is also moved to positive electrode at opposite direction of charging process through external circuit outside the battery for compensating the balance reaction. In addition, the negative electrode for rechargeable LIB is defined as anode when it released Li-Ion during discharging and is defined as cathode when it received Li-Ion during charging. Cathode and anode definitions of

rechargeable LIB are depended on the direction of Li-Ion flowing at that electrode.

During charging and discharging operations, Lithium Ions ( $\text{Li}^+$ ) are inserted into or are extracted from the structure of electrodes (also called intercalation layers or host lattice) without changing its crystalline structures. This crystalline structure is suitable for Li-Ion intercalation and de-intercalation. These operation processes are called the intercalation mechanism. Due to the invariability of the structure during operations, this battery type is safe for operation. However, the reactions of Li-Ion intercalation and de-intercalation are onerous for aging battery. They can lead to a gradual decrease of the capacity during cycling. [8-10].

In addition, the electrodes are separated by a polymer separator, which has a structure as a porous membrane. A separator is used to prevent the electrical short circuits between electrodes while only allowing reversible ionic charge transportation. During intercalation, only Li-Ion can transport via the Lithium salt electrolyte, Lithium hexafluorophosphate ( $\text{LiPF}_6$ ). The property of a good electrolyte is high ionic conduction and high electronic insulation. The electrolyte conductivity depends on the electrolyte temperature and organic solvents. The conductivity increases with increasing temperature. However, the electrolyte solution is unstable when the temperature is up to  $60^\circ\text{C}$  and its conductivity is decreased when the temperature is up to  $80^\circ\text{C}$ . Electrolyte can dissolve in organic solvents as Ethyl Methyl Carbonate (EMC) and co-solvent, Ethylene Carbonate (EC). EC is used to form a solid electrolyte interface (SEI) on the surface of negative side. SEI acts as a protective layer to protect the solvent molecules entering the graphite electrode. For effective protection, SEI must be operated under cell temperature below  $70^\circ\text{C}$  [11-14].

In order to explain the effects from the changing of LIB temperatures during operation, comprehending of the ionic transition between the electrodes via electrolyte is essential. The variation of the internal resistances is referred to the changing of ionic and electrical conductivities of electrolyte. A phase transition of  $\text{LiMn}_2\text{O}_4$  during intercalation and de-intercalation processes, which is a reversibility between cubic (Fd3m) and orthorhombic (Fddd) forms, is a key component in changing electrical conduction of  $\text{LiMn}_2\text{O}_4$ . The effective phase transition of  $\text{LiMn}_2\text{O}_4$  exhibits an increment in electrical conductivity for room temperature operation. However, the electrical conductivity will also be reduced at low temperature [15].

## 2.2. Transient response model and the related parameters

The equivalent circuit modeling in this paper is based on the transient response model of battery. The second order Randle's equivalent circuit model, which was originally proposed for the lead acid battery, is applied. This model will be considered with practical testing information to study the chemical phenomena through the electrical components.

Transient response model of battery as shown in Fig.2 comprises four components:

- The voltage source, called open circuit voltage ( $V_{\text{OCV}}$ ), displays the unique characteristic property of electrodes for each battery type. The  $V_{\text{OCV}}$  is generally indicated as the function of the state of charge (SOC). Details for the  $V_{\text{OCV}}$  will be explained in the next section.
- The bulk ohmic resistances of the cell called effective series resistance (ESR or  $R_0$ ), which consists of resistances of the electrodes, separator, and electrolyte.
- The first RC parallel circuit reflects the faradic charge-transfer resistance (FCTR or  $R_1$ ) and its related double-layer capacitance ( $C_1$ ).
- The second RC parallel circuit reflects the resistance ( $R_2$ ) and capacitance ( $C_2$ ) for the diffusion process in electrolyte [16].

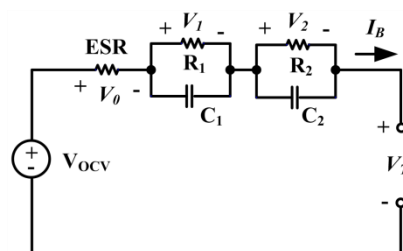


Fig. 2. Transient response model of battery.

In order to study and understand the battery behaviors, the study of related parameters under various operating conditions is needed. For the scope of this study, we intensively focus on the characteristic changes of effective series resistance (ESR) because its variation is greatly influenced by the chemical processes inside battery [17].

## 3. Testing and Proposed Parameter Extraction Methods

In this section, the details for cell test system, dynamic voltage behavior observation, test procedure, and parameter extraction method are introduced.

### 3.1. Cell for testing and test system preparation

In this paper, the Mn-type Li-Ion cell from the NEC Tokin Corporation is used for studying the characteristics and

extracting the parameters. The cell specification is shown in Table 1. The configuration of cell test system is illustrated in Fig. 3.

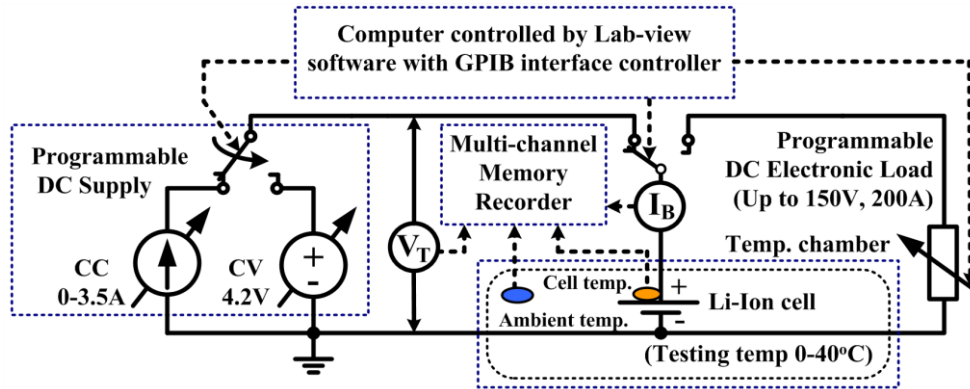


Fig. 3. Cell test system.

Table 1. Cell specification.

Description		Specification
Cell type	Single cell	LiMn <sub>2</sub> O <sub>4</sub>
Rated capacity		3.5Ah
Terminal voltage	Nominal value	3.8V
	Rated charging	4.2V
	Rated discharging	3.0V
Maximum continuous current	Charging	3.5A
	Discharging	20.0A
Operating temperature	Charging range	0 to 40° C
	Discharging range	-10 to 50° C

From Fig. 3, the test system is set up and developed in our laboratory. It consists of the fully programmable power supply with constant current (CC) and constant voltage (CV) functions for charging the cell, fully programmable electronic load for discharging, 30A-current sensor, and the multi-channel memory recorder for recording the terminal voltage, current, and environment and case temperatures of the cell. They are controlled by Lab-view software with a general-purpose interface bus (GPIB) controller. A programmable temperature chamber is used for controlling the ambient temperature of the cell during test between 0°C and 40°C. This test system is used to control and record the practical information for parameter extraction and characterization the dynamic behaviors of the LIB.

### 3.2. Dynamic voltage behaviors of LIB

The dynamic voltage behaviors of LIB can be observed by performing the pulse discharge test using the test system. The dynamic voltage behaviors from the test will be used to explain the voltage response as shown in Fig. 4.

After applying discharge pulse current, the voltage at terminals of battery is instantaneously dropped down as illustrated on the green line. This immediate drop phenomenon is called the instantaneous response from voltage drop ( $V_0$ ) across the equivalent bulk resistance (ESR).

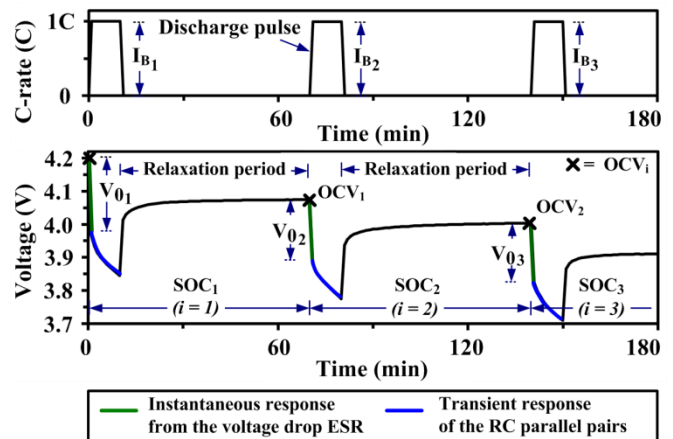


Fig. 4. Dynamic voltage behaviors of LIB from pulse discharging test

The depth of voltage drop depends on the ohmic equivalent resistances of the electrolyte, separator, and electrodes of the battery. After instantaneous voltage drop by continuously applying the discharging current, the voltage gradually decreases over time as illustrated on the blue line in Fig. 4. This smooth change is called the transient response, which is influenced by the voltage drop across the equivalent RC parallel pairs of the circuit in Fig. 2.

After pausing the pulse current or disconnected the battery, the terminal voltage will be relaxed for balancing the internal chemical process called relaxation as illustrated on the black line in Fig. 4. At the end of the relaxation period for each pulse after long resting enough, which means steady terminal voltage and no current flow, the cell has reached equilibrium. Then, the voltage measured across the cell terminals can assume to be the open circuit voltage ( $V_{OCV}$ )

However, for observing the dynamic voltage behaviors in charging process, the test is performed similar to the process of discharging. It is replaced by the charging current instead.

### 3.3. Test procedure and the parameter extraction method

The procedure of cell testing for parameter extraction is started from cell preparation. Before performing the test, the cell must be fully charged at CC-CV mode (3.5A and 4.2V) with controlled ambient temperature of 20°C. Then, the precise pulse discharging tests are performed by applying the periodic constant current, 1C-rate (3.5A), using the programmable test system as aforementioned. The periods of discharge pulse are divided precisely into 3 sections:

➤ The first section is 10 shots 0.6 minutes 1C-rate pulse discharge, which is a high SOC range from 100% to 90% and

the respective pulse deserves as 1% SOC reduction after discharging.

➤ The second section is 16 shots 3 minutes 1C-rate pulse discharge, which is a medium SOC range from 90% to 10% and the respective pulse deserves as 5% SOC reduction.

➤ The last section is 10 shots 0.6 minutes 1C-rate pulse discharge, which is a low SOC range below 10% and the respective pulse deserves as 1% SOC reduction same as the first one.

The pulse discharging tests are started from the full charged at rated charge voltage (4.2V) and continued until the voltage at terminals undergoes the rated cut-off discharge voltage (3V). During the tests, cell is also controlled the ambient temperature at 20°C. For each pulse test, the cell is relaxed for 1 hour.

The sampling-interval for recording terminal voltage and current is set to 20mS/sampling. It is precise enough for observing the instantaneous and transient responses for pulse tests. The details of discharge pulse periods and the battery voltage response are shown in Fig. 5.

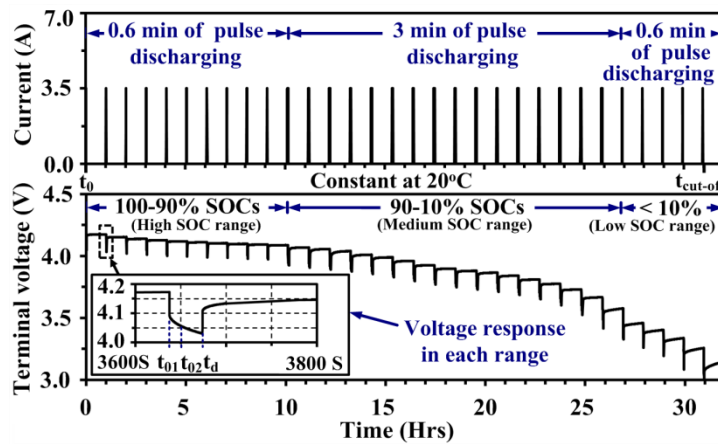


Fig. 5. The battery voltage response to precise pulse discharge test for parameter extraction.

From the transient response model in Fig. 2, we can extract the battery parameters using Eq. (1) to (4). Eq. (1) illustrates the voltage drop summation inside the battery. Eq. (2) is used to calculate the equivalent bulk resistance after immediate applying the discharge pulse from instantaneous response. Eq. (3) and (4) are the solution for the differential equations of two-RC parallel circuits. They are also used to explain the related behavior of transient response inside the LIB.

$$V_{T_i} = V_{OCV_i} - I_{B_i} R_{0_i} - V_{1_i} - V_{2_i} \quad (1)$$

$$ESR_i = V_{0_i} / I_{B_i} \quad (2)$$

$$V_{1_i} = I_{B_i} R_{1_i} (e^{-(t-t_{01})/\tau_{1i}}) \quad (3)$$

$$V_{2_i} = I_{B_i} R_{2_i} (e^{-(t-t_{02})/\tau_{2i}}) \quad (4)$$

Where  $i$  is the experiment number for each SOC reduction,  $V_{T_i}$  is the terminal voltage (V),  $I_{B_i}$  is the battery current (A),  $ESR_i$ ,  $R_{1_i}$  and  $R_{2_i}$  are the effective series,

faradic charge-transfer, and ionic diffusion resistances ( $\Omega$ ),  $V_{OCV_i}$  is an open circuit voltage as function of SOC (V),  $V_{0i}$ ,  $V_{1i}$  and  $V_{2i}$  are the voltage drop (V) for  $ESR_i$ ,  $R_{1i}$ , and  $R_{2i}$  at definite time  $t_{01i}$ ,  $t_{01i}$  to  $t_{02i}$ , and  $t_{02i}$  to  $t_{di}$  (Sec) respectively,  $t_{01i}$  and  $t_{02i}$  are the initial time (sec) of  $V_{1i}$  and  $V_{2i}$  from the experiment,  $\tau_{1i}$  is a short-term time constant (sec) that reflects the transient response of faradic charge-transfer resistance and its related double-layer capacitance [18], and  $\tau_{2i}$  is a long-term time constant (sec) that reflects the

transient response of diffusion phenomenon ( $\tau_{1i} = R_{1i}C_{1i}$  and  $\tau_{2i} = R_{2i}C_{2i}$ ).

Proposed parameter extraction method is based on the method from [18], which only tested and extracted the parameters at 50% of SOC. However, in this paper, the tested SOC ranges are divided more precisely into 3 sections as abovementioned. The parameters of ESR,  $R_1$ ,  $R_2$ ,  $C_1$ , and  $C_2$  are extracted from the tested responses. Calculation steps for parameter extraction based on the experiment of transient response are concluded as illustrated in Fig. 6.

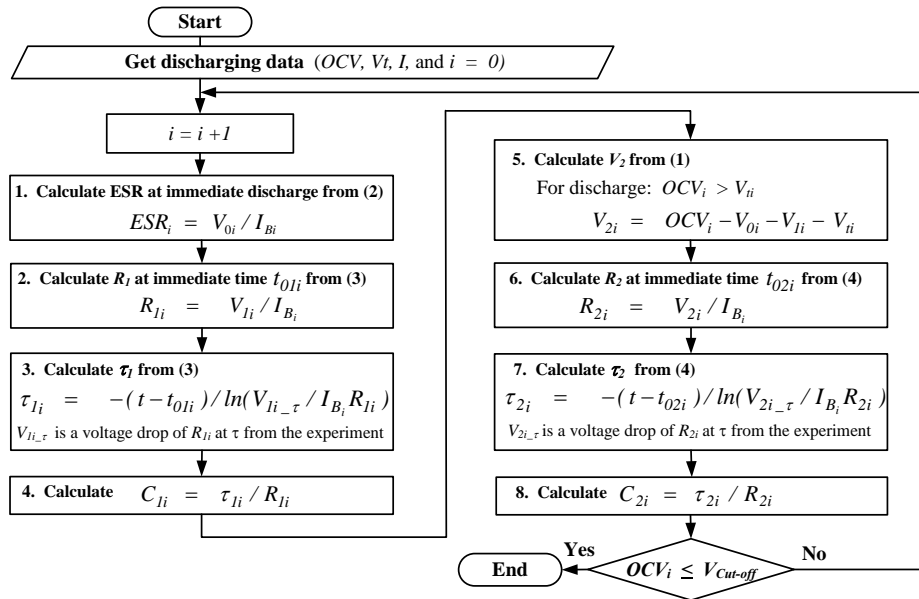


Fig. 6. Flowchart of the proposed parameter extraction method.

From the flowchart in Fig. 6, we can extract the parameters for each SOC range. The average values of the extracted parameters ESR,  $R_1$ ,  $R_2$ ,  $C_1$ , and  $C_2$  are 14.775 m $\Omega$ , 7.935 m $\Omega$ , 10.021 m $\Omega$ , 4.937F, and 1,989.813F respectively. All parameters will be validated in Section 4.

In order to study the battery characteristics and observe them in function of the state of charge (SOC), the coulomb-counting method is used. The SOC of battery is calculated from the measured cumulative current by Eq. (5). It defined as the charge available at that point to the total charge available when the cell is fully charged. The accumulated battery capacity ( $Q_{acc}$ ) in Ah, and the capacity deterioration ( $Q_d$ ) are evaluated by Eq. (6) and Eq. (7), respectively, for studying the battery behaviors under various environment temperatures and C-rates.

$$SOC(t) = SOC_0 - \int_{t_0}^{t_{cut-off}} \frac{i(t)}{3600 \times Q_{rated}} dt \quad (5)$$

$$Q_{acc} = \frac{1}{3600} \int_{t_0}^{t_{cut-off}} i(t) dt \quad (6)$$

$$Q_d = ((Q_{acc} - Q_{rated}) / Q_{rated}) \times 100 \quad (7)$$

Where  $SOC_0$  is the initial value of SOC,  $SOC(t)$  is the state of charge of battery from the time at starting the test ( $t_0$ ) to the time at rated cut-off voltage ( $t_{cut-off}$ ),  $Q_{rated}$  is a rated capacity of the battery (Ah), and  $Q_d$  is the capacity deterioration by operation (%).

#### 4. The Modeling for Parameter Verification

The extracted parameters from the transient response model following the proposed extraction method from Fig. 6 should be verified before studying the battery behaviors. In this case, we refer to the applied transient response equivalent circuit model for parameter verification as shown the details in Fig. 7.

##### 4.1. Equivalent circuit model

From Fig. 7, the applied transient response equivalent circuit model comprises the state of charge voltage model

based on the equivalent battery capacity (Left part of the circuit) and voltage-current characteristics model (Right part of the circuit) based on [19] considering with our practical testing information. The model is used for verification of extracted parameters in Section 3. This model is implemented in a Spice simulation.

In case of the equivalent battery capacity based state of charge voltage model in Fig. 7, the current controlled current source (CCCS<sub>1</sub>) represents the battery current varying with the load to reflect the state of charge voltage (V<sub>SOC</sub>) of the battery.

Self-discharge resistance (R<sub>sd</sub>) represents the battery leakage. Usually, the rate of self-discharging is calculated per month. This self discharge can be determined using the long term experiments by comparing the RC-natural response voltage before and after taking long resting when it is disconnected. For this battery, it is less than 3% per month. Then, the self-discharge resistance will be ignored by setting to infinity.

The next component is the equivalent capacitance (C<sub>eqv</sub>). It is defined as an initial equivalent capacity of LIB that is used for maintenance the battery voltage from the rated voltage to

full cut-off discharged voltage of battery at standard condition (1C-rate, 20°C). The equivalent capacitance and the rated energy of LIB can be expressed as shown in Eq. (8) and (9), respectively.

$$C_{eqv} = 2W_C / (V_{rated}^2 - V_{cut-off}^2) \tag{8}$$

$$W_C = V_{rated} I_{rated} t \tag{9}$$

Where C<sub>eqv</sub> is the equivalent capacitance of the battery (F), W<sub>C</sub> is the rated energy of the equivalent capacitance (J), V<sub>rated</sub> is the rated nominal voltage of the battery (V), V<sub>cut-off</sub> is the discharge cut-off voltage of the battery (V), I<sub>rated</sub> is the rated operating current of the battery (A), and t is the time period for battery operation (Sec).

In the meantime, for the voltage-current characteristics model in Fig. 7, the voltage controlled voltage source (VCVS<sub>1</sub>) represents the open circuit voltage of LIB in function of the SOC. The elements ESR, R<sub>1</sub>, C<sub>1</sub>, R<sub>2</sub>, and C<sub>2</sub> are the extracted parameters that are also set in the Spice simulation program. These extracted parameters are verified by observing the voltage response at the terminals of LIB.

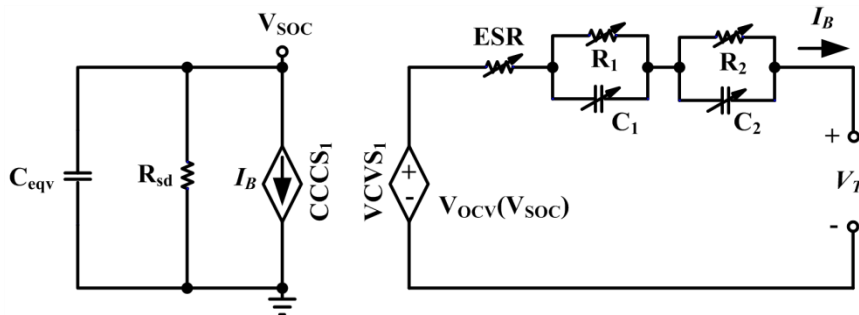


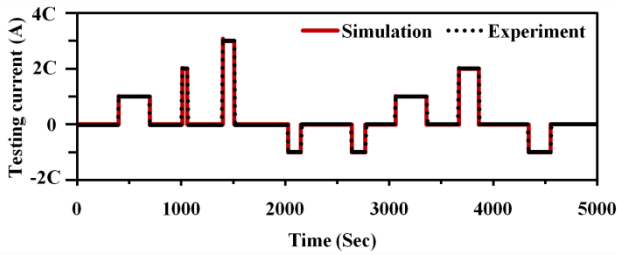
Fig. 7. The applied transient response equivalent circuit model for parameter verification.

#### 4.2. Parameter verification

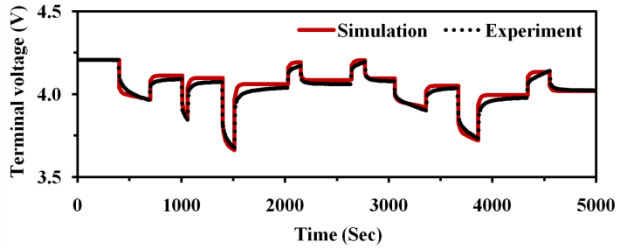
For the parameter verification, we set up the new experiment using the same test system. The pulse currents are injected into the testing cell terminals with the different amplitudes and periods of pulse currents between -1C and 3C, for charging and discharging respectively. Then, the voltage response behaviors at the testing cell terminals are recorded. Next, the extracted parameters from the proposed extraction method are set in a Spice simulation program referred by Fig. 7. The simulated pulse currents with the same amplitudes and periods as in the experiment are also set and injected into the battery terminals of the circuit in simulation program. The pattern details and the comparison between simulation and experiment of testing current can be seen in Fig. 8a. A comparison of voltage response behaviors between simulation

and experimental results is illustrated in Fig. 8b. Fig. 8b is the comparative result that shows an acceptable conformity of the terminal voltage response between the experiment and simulation. The error pattern of voltage response behavior between the experiment and simulation result can be observed in Fig. 8c.

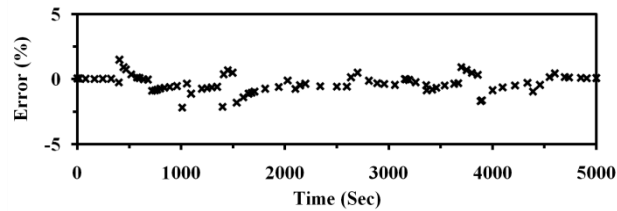
The errors and standard deviations between the experiment and simulation result are summarized in Table 2. These results lead us to understand the terminal voltage behaviors of battery with the chemical reaction variation.



(a) The testing currents.



(b) The voltage response.



(c) The errors of voltage response behaviors between the experiment and simulation result.

**Fig. 8.** Comparison between the experiment and simulation result for the parameter verification.

**Table 2.** The errors and standard deviations (S.D.) between the experiment and simulation.

Error of	Max.	Min.	Average
simulated voltage	1.483 %	-2.173 %	-0.332 %
S.D. of voltage response			26.26 mV
S.D. of error			0.664%

## 5. Battery Characteristic Results

### 5.1. Open circuit voltage characteristics

This section characterizes an OCV as a function of SOC. The OCV characteristic is different for each battery type. It has a unique character that reflects the electrode property. In practical operation, the OCV is defined as the voltage across the battery terminals at steady state after disconnecting the battery from the load (even the charger) and taking long resting period for its internal chemical process relaxation to its equilibrium. In this paper, we rest the battery for 1 hour after applying each constant pulse current (1C-rate at 20°C) as described in Section 3.

Usually, the OCV has a non-linear relationship with the SOC. In this study, we ignore the OCV hysteresis effect by averaging the OCVs from charging and discharging. The criteria for modeling the OCV is to simplify into the linear model, but precise enough for studying or investigating the characteristic. Thus, OCV linearized model will be introduced.

The linearization ranges of SOC are divided into 20-80%, 20-90%, 15-95%, and 10-95% respectively for evaluating the applicability and the appropriate range for OCV linearized model. This is used for considering the appropriate linear model fitting range. Then the residual sum of squares (RSS) and error for each range are evaluated as shown in Fig. 9. The appropriate SOC range for linearization is 15-95%. Because it gives the RSS only 0.00178 V<sup>2</sup> and the SOC linear range is wide enough for observing the OCV response when compared to the widest range, with the highest RSS of 0.01416 V<sup>2</sup>, as 10-95%. The linearized OCV model in the range of 15-95% SOC is shown in Eq. (10).

$$OCV(SOC) = (4.5036 \times 10^{-3}) SOC + 3.690 \quad (10)$$

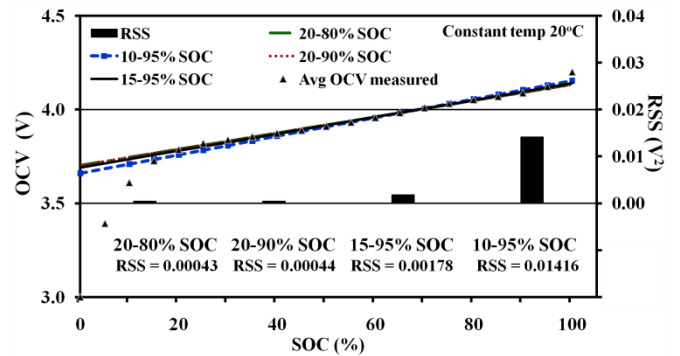


**Fig. 9.** OCV characteristic and the comparison of RSSs for different linearization ranges.

### 5.2. Effective series resistance characteristics

The design of testing for studying the effective series resistance (ESR) characteristics is based on the limitation of cell specification as detailed in Table 1. All ESR characteristics are observed from the instantaneous response of voltage drop (V<sub>0</sub>) at the terminals of the cell as described in Section 3. Before each discharging test, the cell is fully charged at standard condition, 1.0C at 20°C following CC-CV method and before each charging test, the cell is also discharged to a cut-off voltage at standard condition. In case of studying the effects of C-rates to ESR characteristic, these pulses charging and discharging tests are performed for the different C-rates between 0.1C and 1.0C at 20°C.

In case of studying the effects on temperatures to ESR, the pulse charging and discharging tests are also applied for 10



minutes for the different ambient temperatures between 0°C and 40°C with constant current 1C-rate in the testing chamber. The resting period for each pulse test is 1 hour. After the pulse tests, the effective series resistances can be obtained by using Eq. (2). The effects on C-rates and temperatures to ESR are illustrated in Fig. 10 and 11, respectively.

Fig. 10 shows the characteristics of ESR to C-rates. For all of different C-rates, the resistance has not obviously changed and almost constant in the range of 15-95% SOC. We can conclude that the variation of C-rates under constant temperature does not affect to the ESR.

Fig. 11 also shows the significant characteristics of ESR to temperatures. For all of different temperatures, the resistance is also constant along the range of 15-95% SOC. However, for the SOC range below than 15%, the resistances have increased. They have much more different with the decrement of temperature. Under low temperature condition, the viscosity of electrolyte is high that makes Li-Ion difficult to transport between the electrodes during intercalation mechanism. This raising of electrolyte resistance reflected to the increment of ESR.

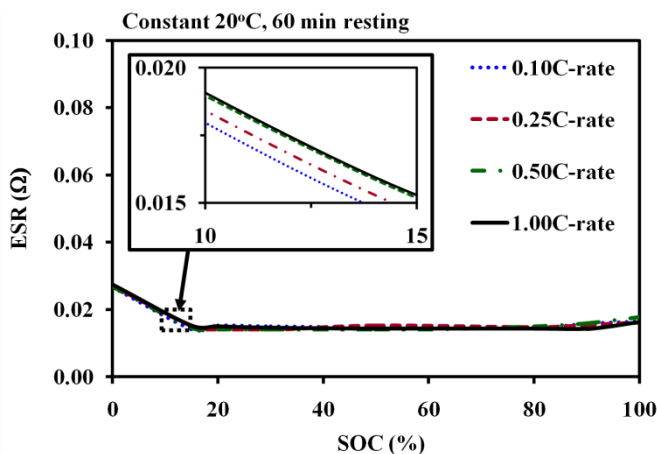


Fig. 10. ESR characteristics under different C-rates.

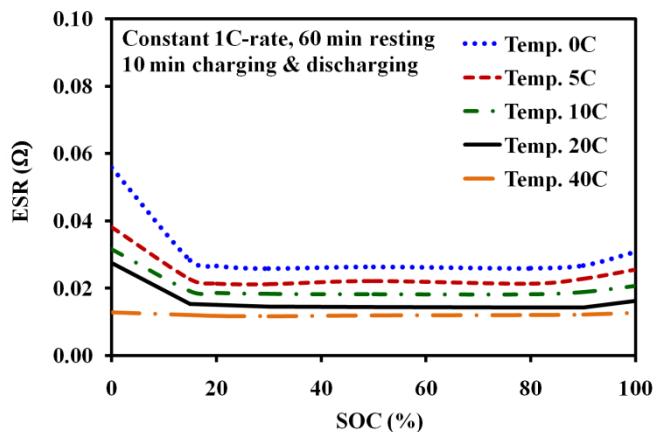


Fig. 11. ESR characteristics under different temperatures.

The relationship under low temperature between the ESR (also FCTR) and the ionic conductivity of the electrolyte is also reported in [20].

The relationship between the ESR and operating temperature is shown in Fig. 12. For all SOC ranges, the variation of resistance to temperature is low for operating temperature higher than 10°C. For decrement of temperature, the ESRs exhibit the gradual increasing trend. Furthermore, when we plot the ESRs at different SOC ranges, the ESR for 0% SOC is obviously high, at the lowest temperature as 0°C, the ESR increases by 1.66 times. This can be explained in term of discharged state, or immediate starting of charge from the battery cut-off state, especially at low temperature. These states are the most viscous for Li-Ion movement during starting in the intercalation process from the reason as aforementioned. The ESR model as a function of operating temperature ( $T_0$ ) at constant 1C-rate is illustrated in Eq. (11).

$$ESR(T_0) = 2.75336 \times 10^{-2} \cdot e^{(-2.46976 \times 10^{-2})T_0} \quad (11)$$

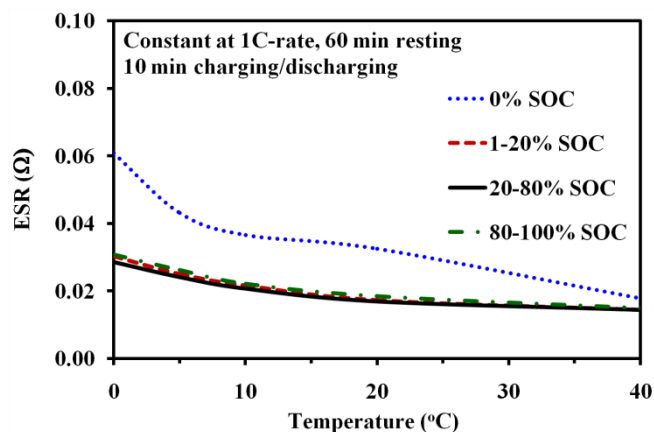


Fig. 12. The relationship between the ESR and operating temperature at different SOC ranges.

### 5.3. Capacity characteristics

In this section, the capacity characteristics for Mn-LIB are analyzed and evaluated. The test parameters as C-rates and temperatures are used for evaluating the operational and environmental conditions. They are from 0.5C to 5.0C-rates and from 0°C to 40°C respectively. The same test system as illustrated in Fig. 3 is used for discharge tests following the method from [21], which discharges a fully charged cell limited by the rated charging and discharging of cell voltages from 4.20V to 3.00V. The accumulated battery capacities are

calculated based on the measured cumulative terminal currents by using Eq. (6) for various temperatures and C-rates. These capacity characteristic results are illustrated in Fig. 13.

From Fig. 13, all cell capacity characteristics increase with the increase of SOC and have a linear relationship for each C-rate of discharge continuous constant current. The changing of operating temperatures does not obviously affect on the cell capacity for low C-rate as shown in Fig. 13a. However, the reduction of the effective capacity is visually obvious when the C-rate is increased and the temperature was dropping as shown in Fig. 13b-13d respectively.

The effect of temperatures to the cell capacity at various C-rates is shown in Fig. 14 and the effect of C-rates to the deterioration of cell capacity at various temperatures is shown in Fig. 15. The capacity deterioration for life cycles is far from the scope of this paper. However, the details of lifetime to capacity fading are reported in [21].

In Fig. 14, the effective capacity is not affected by the temperatures at low discharging rates. However, for high

discharging rates, the trend of cell capacity characteristics has more dropped down with decreasing temperature. These characteristics can be explained by the chemical reaction inside battery. During discharging under low temperature, the electrolyte resistance is high due to the reduced ionic conductivity in the electrolyte. In this case, the Li-Ion transportation between electrodes in the electrolyte is more difficult.

Next, consider the effects of C-rate to the effective capacity during operation at high C-rate under constant temperature, the Li-Ion transportation rate is increased and exceeds the rate that Li-Ion can be fully intercalated into the intercalation layers [22]. Under these conditions, the exceeding Li-Ion may temporarily accumulate on the surface of electrode. Whenever the Li-Ion cell operates under low temperature and high C-rate conditions, the abilities of Li-Ion releasing and insertion between electrodes are also reduced. These operations result in the significant deterioration of the battery capacities.

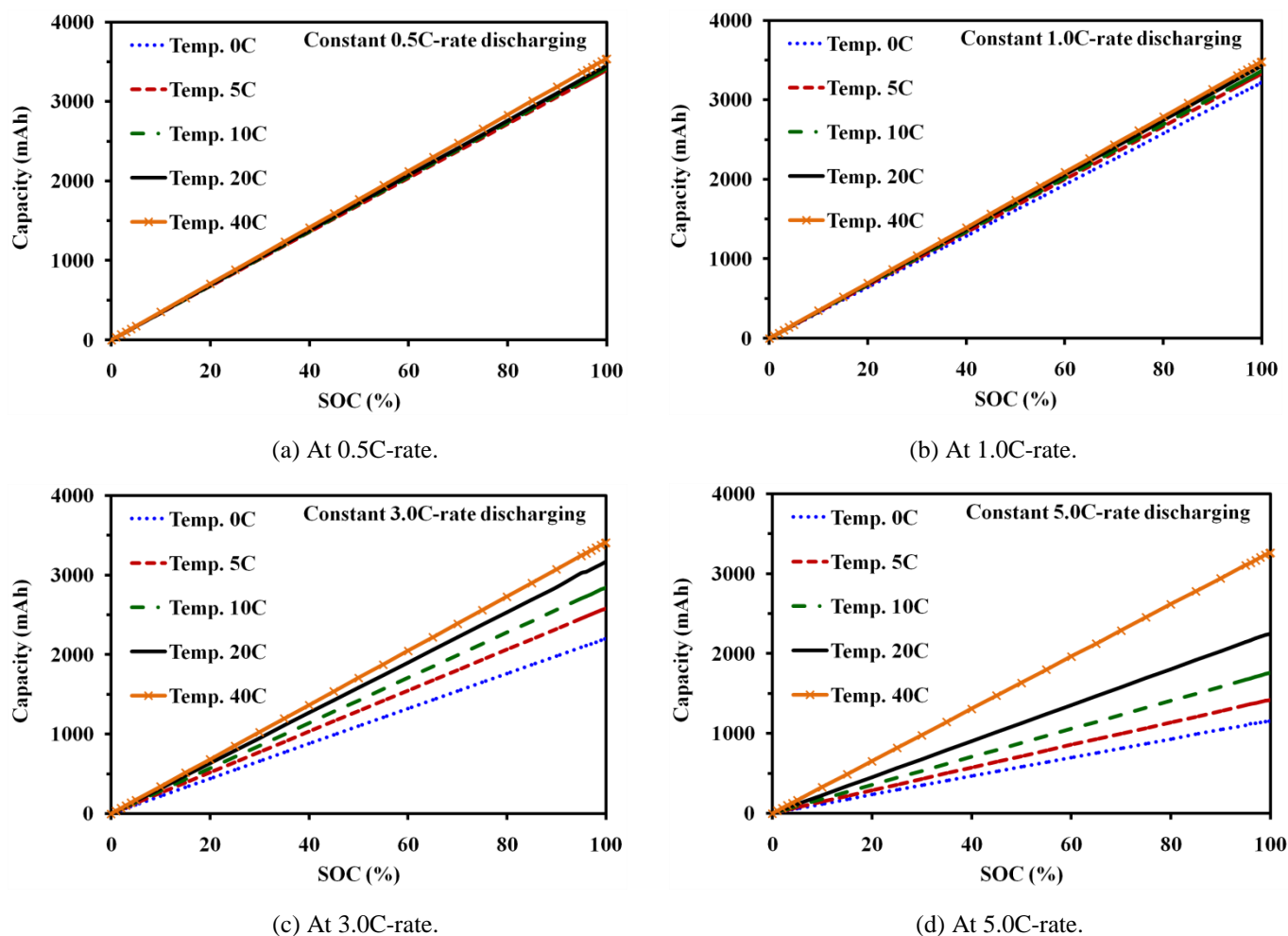


Fig. 13. Effect of incremental C-rates to cell capacity under various temperatures

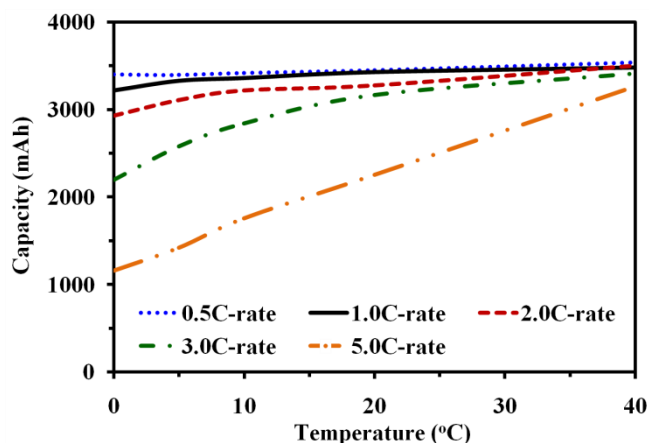


Fig. 14. Effect of temperatures to the cell capacity at various C-rates.

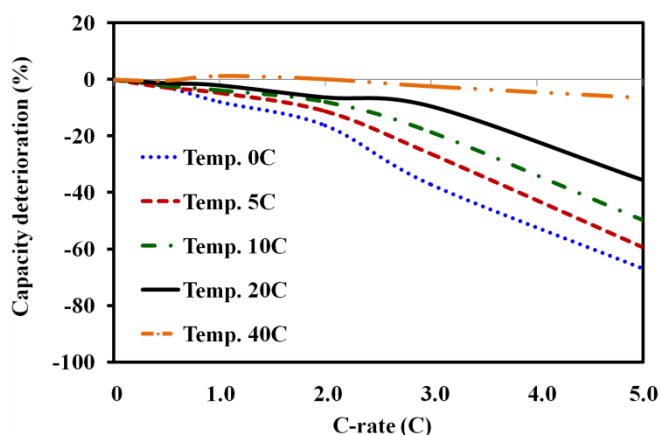


Fig. 15. Effect of C-rates to the deterioration of the cell capacity at various temperatures.

The experimental results in Fig. 15 indicate all these phenomena as abovementioned. A maximum capacity deterioration of this Mn-LIB, occurred at the highest C-rate and the lowest temperature (5C-rate, 0°C), is 68.87%. These results led us understand the effects of the operational and environmental conditions to the cell capacity deterioration.

## 6. Conclusion

This paper proposed the parameter extraction method based on the experiment of transient response and studied the electrical characteristics for Manganese-type Lithium-Ion battery under various operating conditions. The proposed extraction method including the introduction of test system and calculating procedure can be applied for extracting the parameters for any types of Lithium-Ion battery that have similar transient response behavior.

The parameters received from this proposed extraction method were validated in the simulated transient response model with an acceptable result by compared with the experiment under the same condition. The simulated dynamic voltage of this model can be used for studying and predicting the response behavior of battery terminal voltage to the

variation of applied terminal current before the worst-case occurrence such as over current or over voltage phenomena.

From the studies, we also found that at high SOC, the ESR is insensitive to operating currents under constant temperature. However, it will increase when the temperature decreases, especially at low SOC. Under low temperature, high viscosity of electrolyte causes to reduce the ionic conductivity and reflects to the increment of ESR. The capacity deterioration in LIB is greatly affected by the temperature and operating current. It will be obviously increased when the battery operates under low temperature and large current.

These study results let us understand the characteristic behaviors of the battery under different conditions of temperatures and operating currents including the capacity deterioration characteristics. These results can also be the fundamental guideline for engineers who want to design the renewable energy storage system with Li-ion batteries and their management system and/or the battery protection system in order to determine the optimal operating conditions for this battery type.

In the next step, a development of accurate model for this battery type with practical testing information and the investigation of life cycles to capacity deterioration under various operating conditions should be performed.

## References

- [1] W. Schalkwijk and B. Scrosati, *Advances in Lithium-Ion batteries*, Springer, 2002.
- [2] H. Zhang and M. Y. Chow, "Comprehensive dynamic battery modeling for PHEV applications", *Power and Energy society general meeting, 2010-IEEE*, DOI: 10.1109/PES.2010.5590108, pp. 1-6, 2010.
- [3] Y. Zhang, C. Zhang, and N. Cui, "An adaptive estimation scheme for open-circuit voltage of power Lithium-Ion battery", *Research article in Abstract and applied analysis*, Hindawi publishing corp., Vol.2013, Article ID 481976, pp.1-6, 2013.
- [4] A. Rahmoun and H. Biechl, "Modelling of Li-ion batteries using equivalent circuit diagrams", *Electrical review*, ISSN 0033-2097, R.88NR-7b, pp.152-156, 2012.
- [5] D. Andrea, *Battery management systems for large Li-ion battery packs*, Artech house press, Boston, 2010.
- [6] D. K. Kim, P. Muralidharan, H.W. Lee, R. Ruffo, Y. Yang, Candace K. Chan, H. Peng, Robert A. Huggins and Yi Cui, "Spinel LiMn<sub>2</sub>O<sub>4</sub> nanorods as Lithium ion battery cathodes", *Nano letters*, American chemical society, Vol.8(11), pp.3948- 3952, Dec, 2008.
- [7] A. Patil, V. Patil, D. W. Shin, J. W. Choi, D. S. Paik, and S. J. Yoon, "Review issue and challenges facing rechargeable thin film Lithium batteries", *Materials research bulletin 43 on Science direct*, pp.1913-1942, Sep, 2008.

- [8] T. Piao, S. M. Parka, C. H. Dohb, and S. I. Moon, "Intercalation of Li-ion into Graphite electrodes studied by AC impedance measurements", *J. Electrochem. Sci.*, Vol.146(8), pp.2794-2798, 1999.
- [9] M. Urbain, M. Hinaje, S. Raël, B. Davat, and P. Desprez, "Energetical modeling of Li-ion batteries", *Industry Applications Conf.*, 42<sup>nd</sup> IAS Annual Meeting conference of IEEE, LA, USA, pp. 714-721, 2007.
- [10] G. W. Ling, X. Zhu, Y. B. He1, Q. S. Song, B. Li, Y. J. Li, Q. H. Yang, and Z. Y. Tang, "Structural and thermal stabilities of spinel  $\text{LiMn}_2\text{O}_4$  materials under commercial power batteries cycling and abusive conditions", *Int. J. Electrochem. Sci.*, Vol.7, pp.2455-2467, 2012.
- [11] P. Arora and Z. J. Zhang, "Battery Separators", *Chemical Reviews*, Vol.104(10), pp.4419-4462, 2004.
- [12] H.J. Bergveld, W.S. Kruijt, and Peter H. L. Notten, *Battery management systems: Design by modeling*, Philips research vol.1, Springer, pp.31-52, 2002.
- [13] C. H. Doh, D. H. Kim, J. H. Lee, D. J. Lee, B. S. Jin, H. S. Kim, S. I. Moon, Y. Hwang, and A. Veluchamy, "Thermal behavior of  $\text{Li}_x\text{CoO}_2$  cathode and disruption of solid electrolyte interphase film", *Bull. Korean Chem. Soc.*, 30 (4), pp.783-786, 2009.
- [14] M.B. Pinson and M. Z. Bazant, "Theory of SEI formation in rechargeable batteries: Capacity fade, accelerated aging and lifetime prediction", *Dept. of Physics, MIT, USA*, pp.3-5, 2012.
- [15] M. Parka, X. Zhanga, M. Chunga, G. B. Lessa, and A. M. Sastry, "A review of conduction phenomena in Li-ion batteries", *J. Power sources*, Vol.195(24), pp.7904-7929, 2010.
- [16] E. Kuhn, C. Forgez, P. Lagonotte, and G. Friedrich, "Modelling Ni-MH battery using Cauer and Foster structures", *J. Power Sources*, Vol.58(2), pp. 1490-1497, 2006.
- [17] S.S. Zhang, K. Xu, and T.R. Jow, "Electrochemical impedance study on the low temperature of Li-ion batteries", *Electrochim. Acta*, Vol.49(7), pp.1057-1061, 2004.
- [18] B. Schweighofer, K. M. Raab, and G. Brasseur, "Modeling of high power automotive batteries by the use of an automated test system", *IEEE trans. on instrumentation and measurement*, Vol.52(4), 2003.
- [19] M. Chen and G.A. Rincon-Mora, "Accurate electrical battery model capable of predicting runtime and I-V performance", *IEEE Trans. On Energy Conversion*, Vol. 21(2), pp.504-511, 2006.
- [20] S.S. Zhang, K. Xu, and T.R. Jow, "The low temperature performance of Li-ion batteries", *J. Power sources*, Vol.115(-), pp.137-140, 2003.
- [21] M.A. Roscher, J. Assfalg, and O. S. Bohlen, "Detection of utilizable capacity deterioration in battery systems", *IEEE Trans. On Vehicular Technology*, Vol. 60(1), pp.98-103, 2011.
- [22] K. Eberman, P. Gomadam, G. Jain, and E. Scott, "Material and design options for avoiding Lithium plating during charging", *ECS Transactions*, Vol. 25(35), pp.47-58, 2010.